Photo-manipulated polyunsaturated fatty acid-doped liposomal hydrogel for flexible photoimmunotherapy

Xinyue Lan
Southern Medical University
Junguang Liang
Southern Medical University
Churan Wen
Southern Medical University
Xiaolong Quan
Southern Medical University
Huimin Lin
Southern Medical University
Qinqin Xu
Southern Medical University
Wei Luo
First People's Hospital of Foshan
Guangyu Yao
Southern Medical University Nanfang Hospital
Dan Zhou
First People's Hospital of Foshan
Meng Yu
yumeng999@smu.edu.cn

Southern Medical University

Research Article

Keywords: photodynamic therapy, immunotherapy, responsive release, immunogenic cell death, liposomal hydrogel

Posted Date: February 22nd, 2023

DOI: https://doi.org/10.21203/rs.3.rs-2577846/v1

Version of Record: A version of this preprint was published at Chinese Chemical Letters on April 1st, 2024.
See the published version at https://doi.org/10.1016/j.cclet.2023.108616.

Abstract

Background

Despite the synergy of immune checkpoint blockade (ICB) therapy and photodynamic therapy (PDT) holds great promise as countermeasures against breast cancer, exploring long-term or flexible short-time therapeutic strategies in “cold” tumors remains great challenge.

Methods

Programmed death-ligand 1 antibody (αPD-L1) and photosensitizer chlorin e6 (Ce6) were loaded in polyunsaturated fatty acid-doped liposomal hydrogel Lp(DHA)@CP Gel for flexible local photoimmunotherapy with merely single-dosed administration. Phototriggered drug release and ROS generation of Lp(DHA)@CP Gel were evaluated *in vitro*. To investigate tumor therapeutic effect, NIR laser of 671 nm was used to irradiate tumor site after a single dose of peritumoral administration of Lp(DHA)@CP Gel of 4T1-bearing mice.

Results

With syringe-injectable and self-healing property, Lp(DHA)@CP Gel showed a photo-triggered release of αPD-L1 repeatedly induced to in situ in response to PDT for at least 11 days. Additionally, Lp(DHA)@CP Gel exhibited prominent antitumor efficacy both *in vitro* and *in vivo*. The on-demand treatment can maximize the patient compliance and safety by adjusting therapeutic behaviors via a photo on-off switch. Furthermore, the immunogenic cell death (ICD) effect of PDT evoked “cold” breast tumor to “hot” one, and then assisted the cascade released αPD-L1 to synergistically boost the immunotherapy.

Conclusion

Lp(DHA)@CP Gel is a flexible medication platform, showing promise in improving the objective response rate of ICB therapy and minimizing its systemic toxicity.

Introduction

Despite significant advances in breast cancer treatment, it is still the major cause of cancer-related death in females worldwide [1]. In recent years, a high-profile treatment, immunotherapy has developed rapidly against tumors [2, 3]. Although many clinical used drugs have inhibited tumor growth and metastasis to some extent, most of them hardly achieve long-term or flexible short-time therapeutic effect with merely single-dosed administration [4, 5]. Hydrogel is composed of crosslinked polymeric networks that can form highly hydrated semisolid materials, which facilitate the drug deposition and sustained release [6–8]. With the continuous development of nanotechnology in the past decades, numerous researchers have

designed various in-situ drug release therapeutic strategies using injectable nanomedicine-loading hydrogels as a drug reservoir [9, 10]. For example, Chen has employed a minimally invasiveness measurement to inhibit tumor growth by local injection of programmed death-ligand 1 antibody (αPD-L1) loaded hydrogel [11]. Luo has also reported an all-in-one and all-in-control gel depot to realize a locally symbiotic mild photothermal-assisted immunotherapy [12]. The high peritumoral drug accumulation is beneficial to taking effect, however the drug release behavior is usually hard to be flexibly adjusted, leading to the unnecessary sustained release of drugs in disease site and accompanied with excessive treatment risks, which are of particular concern in immunotherapy [13, 14]. Therefore, the designing of intelligent antitumor platform with high drug storage capability and adjustable release property is highly desirable.

Recently, hydrogels crosslinked via dynamic covalent bonds attracted extensive attention due to their “smart property” originated from the kinetically controlled structures [15, 16]. In this situation, it has inspired us to propose the on-demand tumor therapeutic hydrogels involving stimuli-responsive drug-carrying nanoparticles to realize the localized accumulation and induced repeatedly release of drugs, thereby decreasing the administration times and avoiding excessive treatment as well as the accompanied side. Previous studies have confirmed that amphiphilic materials with unsaturated structures undergo reversible hydrophobic-hydrophilic structural transitions induced by reactive oxygen species (ROS), contributing to the ROS-responsive on-demand disassembly and the subsequent cargo release of nanoparticles constructed based on these functional materials [17, 18]. In the previous research, we have confirmed that the drug-loaded nanoparticles prepared based on the unsaturated materials, such as lecithin and docosahexaenoic acid (DHA) would be disintegrated in response to the overexpressed intratumoral ROS or highly-produced ROS during photodynamic therapy (PDT) to achieve on-demand drug release [19]. Therefore, it inspired us to combine ROS-induced reversible immune drug release liposomal gel with PDT to achieve light-triggered and spatio-temporally controlled photodynamic-/immuno-cascade therapy after one-dose administration.

Although immunotherapy represented by immune checkpoint blockade (ICB) strategy has shown outstanding advantages in breast cancer, especially triple-negative breast cancer treatment, it is still facing risks such as drug resistance and recurrence [20–23]. However, most of the breast cancer are considered as immunosuppressive “cold” tumors, which are hyposensitive to ICB therapies due to the insufficient tumor-infiltrating lymphocytes (TILs) and rich tumor-promoting macrophages or regulatory T cells (Tregs), and excessive anti-inflammatory cytokines [24, 25]. Many studies have shown that PDT can strengthen ICB therapy by converting a nonimmunogenic “cold” tumor to an immunogenic “hot” tumor [26–28]. The introduction of phototherapy promotes the tumor-associated antigen (TAA) presenting to T cells, activating systemic immune responses thus improving tumor sensitivity to immunotherapy [29, 30]. For example, Zhao et al. designed an immune-enhancing polymer-reinforced liposome to enhance TAA cross-presentating in DCs, and then improving the immunogenic cell death (ICD) associated antitumor efficiency by inducing the tumor cells to expose pro-phagocytic calreticulin and release high mobility group box 1 [31]. Therefore, Combining ICB therapy with PDT denotes a promising strategy to potentiate the immune therapy by transferring tumor immune environment from “cold” to “hot”.

In this work, we fabricated an ROS-responsive liposomal hydrogel loading αPD-L1 (Lp(DHA)@CP Gel) to in situ implant in tumor site as a drug depot for repeatedly long-term photoimmunotherapy. The ROS induced by 671 nm laser irradiation led to tumor cell apoptosis through PDT effect, meanwhile the generated ROS as well causing reversible αPD-L1 release from Lp(DHA)@CP Gel due to the peroxidation of unsaturated membrane materials that lead to disintegrity of liposomes (Scheme 1). Moreover, the immunogenic PDT reversed immune cold tumor into hot one through recruiting effector T cells, and then evoked tumor immunity to assist the cascade released αPD-L1 for synergistic immunotherapy. Notably, Lp(DHA)@CP Gel maximized the synergistic antitumor efficacy on breast tumor-bearing mice by photo-manipulated on-off release of immune drugs. In addition, this flexible medication platform facilitated the on-demand photoimmunotherapy as well as greatly avoiding clinical overtreatment risks on patients.

Methods And Materials

Materials

Phosphatidyl ethanolamine (PE) and Cholesterol (CHO) were purchased from AVT Pharmaceutical Tech Co., Ltd. (Shanghai, China). Docosahexaenoic Acid (DHA) and Chlorin e6 (Ce6) were purchased from Shanghai Macklin Biochemical Co., Ltd. (Shanghai, China). Docosahexaenoic Acid (purity 99%) were purchased from Meryer Chemical Technology Co., Ltd. (Shanghai, China). αPDL1 used for therapy was purchased from BIOCELL Biotech Co., Ltd. (Zhengzhou, China). Annexin V-FITC/Propidium iodide (PI) apoptosis detection kit were purchased from Beyotime Biotech. Inc. (Shanghai, China). 2',7'-dichlorofluorescin diacetate (DCFH-DA) were purchased from Beijing Solarbio Science & Technology Co., Ltd. (China). MTT Cell Proliferation Assay Kit were purchased from Yeasen Biotechnology Co., Ltd. (Shanghai, China). Mouse ELISA Kits were purchased from ABclonal Technology (WuHan, China). Cell culture dishes/plates and centrifuge tubes were obtained from NEST Biotechnology Co., Ltd (Wuxi, China). Other reagents were obtained from Sinopharm Chemical Reagent Co., Ltd. (Shanghai, China) and directly used without further purification.

Preparation and characterization of Lp(DHA)@CP Gel

Ce6 (15 mg), PE (15.3 mg) and DHA(22.3 mg) were added to form the lipid precursor by film dispersion method [32, 33]. Next, the liposomal nanoparticle Ce6-DHA@αPD-L1 was fabricated by dropwise adding the αPD-L1 liquid into the preformed liposomes under sonication. Then the liposomes were embedded into aldehyde modified xanthan gum via Schiff base linkages (1:1) to prepare injectable hydrogel for controlled drug release [34]. The injection experiments were performed using a 1 mL syringe to evaluate the injectability of the Lp(DHA)@CP Gel in vitro. The SEM images of the Lp(DHA)@CP Gel were characterized using a Zeiss Gemini 500 scanning electron microscope. Hydrodynamic size distribution was evaluated using a Zetasizer Nano ZS90 at 25°C. Fourier transformed-infrared spectra (FTIR) were measured on a AVATAR360 (Nicolet, USA) spectrometer. The rheological properties were analyzed by a dynamic stress-controlled rheometer (Kinexus, Malvern). The concentrations of Ce6 and αPD-L1 were determined by UV-vis spectrophotometry.

In vitro ROS and αPD-L1 release

Rhodamine B was used to indicate ROS generation [35]. After the laser irradiation (671 nm, 100 mW/cm^2), different prescription solutions were centrifuged (12000 r, 10 min). The above supernatants containing 0.2 mM rhodamine B was allowed to incubate with H_2O_2 (20 mM) and Fe^{2+} (5 mM) for 5 min. Then, the absorbance change at 550 nm was monitored by UV-vis spectrophotometry because the produced ROS through Fenton reaction could reduce the absorbance of rhodamine B. To measure the phototriggerability of the Gel, irradiation was performed using a 671 nm laser (100 mW/cm^2) at different time periods. The concentration of αPD-L1 released from Lp(DHA)@CP Gel was quantified by UV-vis spectrophotometry.

In vitro cytotoxicity of Lp(DHA)@CP Gel

Mouse breast cancer cells (4T1) were cultured in RMPI-1640 medium (Gibco BRL, Rockville, MD, USA) containing 10% fetal bovine serum (FBS) (Sperikon Life Science & Biotechnology Co., Ltd) and 1% antibiotics (penicillin/streptomycin, 10000 U/mL) at 37°C in an atmosphere of 5% CO_2. To study the synergistic PDT cytotoxicity of Lp(DHA)@CP Gel, 4T1 cells were seeded in 96-well plates at a density of 5×10^3 cells per well and incubated for 24 h, and then submitted to different treatments (different nanoparticle solutions with/without laser irradiation). After 24 h of incubation, the cytotoxicity was determined by MTT assay.

Intracellular ROS generation

The in vitro ROS levels were determined by the fluorescence intensity of the oxidized DCFH-DA by ROS. 4T1 cells were seeded in 6-well plates at a density of 1×10^5 cells per dish for 24 h. After different treatments, the cells were added with DCFH-DA solution (10 μM) and continued incubating for 30 min in the dark. Subsequently, the cells were washed with PBS and submitted for CLSM observation.

In vivo antitumor efficacy

Balb/c female mice with a weight range of 18–20 g (6–8 weeks old) were purchased from animal experiment center of Southern Medical University. The mice were reared in separate cages, fed standard feed and tap water, and the cages were maintained at 25°C. Day and night were alternated for 12 h. All animal experiments were performed under the guidelines evaluated and approved by the ethics committee of Southern Medical University, P. R. China.

Luciferase-transfected 4T1 (4T1-Luc) tumor-bearing Balb/c mice were established by the injection of a suspension of 4T1-Luc tumor cells (1×10^6 cells). As the tumor volume reached 100 mm^3 in volume, 4T1 breast tumor-bearing Balb/c mice were divided into 6 groups (n = 5) for various treatments with (a) NS (Control), (b) Free αPD-L1, (c) Lp(DHA)@C Gel - Laser, (d) Lp(DHA)@CP Gel - Laser, (e) Lp(DHA)@C Gel + Laser, (f) Lp(DHA)@CP Gel + Laser was injected around tumor. Each mouse in corresponding groups was treated with equivalent Gel (1 mg/kg αPD-L1) via peritumoral injection. At days 1, 7, and 14 post injection, the mice were intraperitoneally (i.p.) administered 200 μL of D-Luciferin sodium (50 mg/mL in PBS)

(Sigma-Aldrich), and imaged using the In Vivo Imaging System (Xenogen IVIS 200; PerkinElmer) 10 min post-i.p. injection. The tumor volume was tested every day and calculated by the following equation: (Tumor Length) × (Tumor Width)2/2. The body weights of the mice were weighed every two days as an indicator of systemic toxicity.

The mice were sacrificed at the 14th day for collecting the tumor tissues and major organs (heart, liver, spleen, lung and kidney). These tissues were fixed with 4% paraformaldehyde and sliced for H&E staining. The tumor sections were stained with Ki-67, TUNEL and examined using an Olympus FV1000 confocal microscope.

In vivo antitumor immune response

Freshly harvested tumor tissues were digested with collagenase IV (Sigma-Aldrich) and made into single-cell suspensions according to the manufacturer's instructions. After that, cells were collected and diluted to 1×10^7 cells/mL. 100 μL cells were stained by adding a cocktail of fluorescently conjugated antibodies for flow cytometry analysis (e.g., APC-Cy7 anti-CD3 antibody, APC anti-mouse CD8 antibody, PE anti-mouse CD4 antibody). Furthermore, the pro-inflammatory cytokines from mice sera including IFN-γ, TNF-α, IL-6 and IL-1β were determined by using enzyme-linked immunosorbent assay (ELISA) kits following standard protocols. Further, foxp3, the marker of Treg cells, and f4/80, the marker of macrophage were used to indicate the capability of the immune therapy potentiated by PDT.

Statistical analysis

Results are presented as mean ± standard error of the mean (SEM). The data presented in the figures is rep- resentative of at least three independent experiments unless otherwise stated. All statistical analysis were performed using the Prism software package (PRISM 8, GraphPad Software, USA). One-way analysis of variance (ANOVA) test and t-test were performed for statistical analysis. Statistical significance was set as follows: *P < 0.05, **P < 0.01, ***P < 0.001 and ****P < 0.0001.

Results

Preparation and characterization of Lp(DHA)@CP Gel

The Lp(DHA)@CP were synthesized by film dispersion method with ROS-responsive polyunsaturated fatty acid DHA doped in the liposomal membrane. Lp(DHA)@CP Gel was then formed by mixing with the same volume of aldehyde modified xanthan gum. Figure 1A clearly showed that the Lp(DHA)@CP Gel could be easily extruded through a syringe, and remained immobile and stable in aqueous circumstance. In addition, the hydrogel cutted into two pieces could be fused and recovered to a homogeneous gel along the cutting line. The SEM image shown in Fig. 1B illustrated the polyporous morphology of Lp(DHA)@CP Gel and the spherical shaped Lp(DHA)@CP on the surface of hydrogel. The DLS data confirmed the uniform and nanosized liposomes incorporated in the hydrogel with a particle size of ~ 228 nm and a PDI of 0.107 (Fig. 1C).

The dynamic crosslinking hydrogel network of Lp(DHA)@CP Gel attributed to the construction of Schiff Base bonds between the hydrophilic amino head group of Lp(DHA)@CP and the aldehyde groups of xanthan gum matrix, facilitated its injectable capability. Therefore, FTIR spectra of different hydrogels were characterized to evaluate the synthesis of Schiff Base bonds (Fig. 1D). The FTIR spectrum of Lp(DHA)@CP Gel showed the disappearance of the peak represented for aldehyde group on xanthan gum (v(C = O), 1732 cm^{-1}) [36]. In contrast, the DHA-absent liposomal hydrogel Lp@CP Gel remained the representative aldehyde group peak, verified that the formation of Schiff base bond highly depend on the existence of amino groups on DHA. Moreover, the degradation of liposomes after addition of H_2O_2 did not make any changes of FTIR spectrum, evidenced that the integrity or disassembly of the liposome during the responsive drug release process would not change the hydrogel structure.

The injectable hydrogel was expected to be administrated through syringe and remained in situ to perform long-term therapeutic effect. Therefore, the storage modulus (*G'*) and the loss modulus (*G''*) versus frequency were measured to evaluate the viscoelastic property of the hydrogel materials. The *G'* value was much higher than that of *G''* during the stress from 1 to 20 Pa or the sweeps from 0.5 to 25 rad/s, indicating a representative elastic network in Lp(DHA)@CP Gel (Fig. 1E, F). As expected, when the stress or frequency increased, the *G'* was decreased much more dramatically than that of *G''*, resulted to an obviously lower *G'* value than *G''*, displaying the typical shear-thinning character. The similar property of hydrogel was also found at 25°C and 45°C, indicating the good stability during the storage and application (Fig. S1).

Assessment of Phototriggered Drug Release

The DHA-dependent liposome endowed the Lp(DHA)@CP Gel with the stability in the absence of NIR laser irradiation, meanwhile the responsive αPD-L1 release property under NIR laser exposure, which process could be repeatedly controlled induced by applying or removing the photosource (Fig. 2A). The overall increased absorption and the characteristic peaks of Ce6 at 404 nm and 280 nm in UV-vis spectra provided evidences for the successful construction of Lp(DHA)@CP nanoparticles and the efficient encapsulation of Ce6 (Fig. 2B). Along with the irradiation time, the absorption peak represented for Ce6 was gradually decreased meanwhile another absorption peak at 238 nm represented for lipid peroxide was obviously increased (Fig. 2C), indicated the formation of the conjugated dienes after the lipid peroxidation process [37].

To further investigate the mechanism of phototriggered drug release, liposomal hydrogels prepared with saturated (HSPC) or unsaturated (DHA) lipid materials were to study the ROS generation and αPD-L1 release profiles with or without NIR light irradiation. It was obvious that the liposomal hydrogels were able to produce equivalent ROS amount induced by NIR laser at the same concentration of Ce6 (Fig. 2D). However, only a small portion of αPD-L1 was released from LP(HSPC)@CP Gel triggered by NIR light, while the αPD-L1 release was remarkedly enhanced in LP(DHA)@CP Gel (Fig. 2F). Amongst, DHA-based liposomal gel has significant higher degree of unsaturation compared to those based on EPA, PC and HSPC. No obvious photo-boosted drug release was observed in saturated HSPC-dependent group, while a

significant release inducement was found in monounsaturated EPA and PC groups, and an even more release improvement in polyunsaturated DHA group (Fig. 2G).

As shown in Fig. 2E, Lp(DHA)@CP Gel performed a steady αPD-L1 release after repeatedly triggered for 4 times during over 10 d. In order to simulate the intrinsic ROS level in tumor microenvironment and the controlled ROS level by PDT, H_2O_2 with different concentrations rather than irradiation conditions were given to mimic intrinsic intratumoral conditions. The Lp(DHA)@CP Gel showed a relatively stable drug incorporation in the tumor microenvironment-mimic H_2O_2 conditions, while a significant drug release under the laser irradiation (Fig. S2). Furthermore, despite for the gradual release of αPD-L1 once or repeatedly triggered by the laser or H_2O_2, the hydrogel remained stable and reasonable quality loss in aqueous solutions for over 10 d (Fig. S3, S4), confirmed the excellent stability of Lp(DHA)@CP Gel that met the requirements for the long-term implantable material.

Evaluation of Photo-Responsive Cytotoxicity

In order to investigate whether the therapeutic effect of the Lp(DHA)@CP Gel would be attenuated during repeated inducement after one-time implantation during the medication period, we have evaluated the photo-responsive cytotoxicity under different illumination times. Ce6 contained hydrogels was demonstrated a significant tumor cell killing effect once triggered by NIR laser attributed to the ROS-generation role of Ce6, however the addition of αPD-L1 showed negligible cytotoxicity improvement at both conditions with or without laser exposure (Fig. 3A), which can be explained by that the released αPD-L1 took effects by interfering the reaction between immune cells and tumor cells, rather than directly killing tumor cells. The intracellular ROS generation in 4T1 cells was then indicated using dichlorofluorescein diacetate (DCFH-DA) for CLSM observation. The great level of ROS was only found in Lp(DHA)@C Gel + L and Lp(DHA)@CP Gel + L groups with laser irradiation, again proved that the existence of both Ce6 and laser exposure were necessary for ROS generation, which displayed the direct role on in vitro cytotoxicity (Fig. 3B). The cell apoptosis measured by flow cytometry analysis further confirmed the ROS-dependent tumor cell killing effect (Fig. 3C). The implantable hydrogel was supposed to perform long-term antitumor effect, therefore its cytotoxicity was further assessed under 4 times of 1 min-laser cycles. As shown in Fig. 3D, the cytotoxicity of Lp(DHA)@CP Gel was superimposed with the illumination times, indicating the sustained cytotoxicity during the administration process. The live and dead 4T1 cells with Annexin V/propidium iodide (PI) staining shown in Fig. 3E suggested that Lp(DHA)@CP Gel could induce cell death in response to photo-exposure, which could be strengthened by increasing illumination times.

In vivo anticancer efficacy

The in vivo anticancer efficacy of Lp(DHA)@CP Gel was evaluated on 4T1-luc tumor-bearing BALB/c mice with a one-time implantation and repeated photo-inducement treatment process (Fig. 4A). As the luciferase-labeled 4T1-luc tumors monitored in Fig. 4B, the liposome hydrogels (Lp(DHA)@C Gel and Lp(DHA)@CP Gel) without laser irradiation only exhibited a limited inhibition effect on the tumor growth inhibition compared to control group.

The individual and average tumor growth curves showed that the Lp(DHA)@CP Gel + L showed a tumor volume increase that was distinctly slower than the other groups (Fig. 4C, D). Amongst, two of the mice even exhibited no measurable tumors at the end of the study (Fig. 4E, F). In addition, no obvious body weight loss was observed from mice treated with each intervention (Fig. S5). Histological examinations showed no pathological changes in major organs of mice receiving various treatments (Fig. S6). Tumor tissues were then harvested and stained with H&E and in situ terminal deoxynucleotidyl transferase dUTP nick end labeling (TUNEL) for cell morphology observation and apoptosis analysis. According to the histological examinations (Fig. 4G), the most significant classical apoptotic features including condensed and hyperchromatic nuclei were observed in tumor sections from the Lp(DHA)@CP Gel + L, whereas negligible apoptosis was found from the tumors treated with the other interventions. Further TUNEL staining assay confirmed the significantly elevated apoptotic tumor cells in tissues after treated with Lp(DHA)@CP Gel + L. On the other hand, the proliferation of tumor cells after different treatments was also performed by immunofluorescence Ki-67 staining study. As shown in Fig. 4F, obvious decreased Ki-67 positive tumor cells were observed after treated with Lp(DHA)@C Gel + L and Lp(DHA)@CP Gel + L, indicating the potent effects of Ce6-dependent PDT on elevating apoptosis level and suppressing proliferation of tumor cells.

Evaluation of Photo-Activated Immune Responses

Preclinical studies have shown that local PDT are able to enhance systemic antitumor immunity [38], which is usually mediated by recruiting $CD8^+$ T cells and $CD4^+$ T cells [39]. Considering that the efficiency of ICB strategy is severely limited by the low infiltration of effector T cells, PDT could significantly improve the immunotherapy effect of ICB via dramatically upregulating intratumoral immune cell infiltration. To further prove the mechanism of synergistic anti-tumor immune therapy mediated by Lp(DHA)@CP Gel + L, the immune responses in tumor tissues after different treatments were further studied. The populations of $CD8^+$ T cells and $CD4^+$ T cells were dramatically increased in Lp(DHA)@C Gel + L and Lp(DHA)@CP Gel + L groups (Fig. 5A), validated the effective immune activation by PDT in tumor microenvironment. The elevated intratumor infiltration frequency of $CD8^+$ and $CD4^+$ CTLs examined by flow cytometry better illustrated the immune-assistant role of PDT in the synergistic antitumor performance of Lp(DHA)@CP Gel (Fig. 5B-D).

The immune therapy potentiated by PDT not only through recruiting effector T cells, but also mediated via modulating macrophages. IL-6 and IL-1β and their downstream mechanisms are involved in a variety of autoimmune inflammatory responses, further affect cell proliferation, differentiation and apoptosis [40]. In addition, a productive T cell response against a tumor antigen results in the upregulated expression of interferonγ (IFN-γ) in the tumor microenvironment [41], thus the disruption of tumor cell responses to IFN-γ signaling unnecessarily leads to the resistance mechanism to antitumor immunotherapy, including ICB strategy. Therefore, after receiving PDT treatment mediated by Lp(DHA)@C Gel + L or Lp(DHA)@CP Gel + L, the elevated expression of IL-6, IL-1β and IFN-γ in serum released by immune cells for conversely altering T cell responses are the key biomarkers represented for the comprehensive antitumor immune activation (Fig. 5E, F, G). The immunofluorescence images shown in

Fig. 5I again proved the activation of effector T cells and the down-regulation of immunosuppressive regulatory T (Treg) T cells after the synergistic immunotherapy. Also, the remarkable up-regulation of macrophage infiltration was observed in tumor tissues from mice accept immune treatments combined with Ce6/Laser-dependent PDT. As a positively biomarker that correlates with macrophage infiltration in tumor stroma, TNF-α secretion was also significantly enhanced after receiving Lp(DHA)@CP Gel + L treatment (Fig. 5H) [42]. The immune activation via the recruiting of tumor-inhibiting effector T cell and the suppression of tumor-promoting Treg cells mainly facilitate the long-term tumor inhibition, which was further investigated by the metastasis on the major organs after drug withdrawal (Fig. 5J). The mice treated with Lp(DHA)@CP Gel + L for 2 weeks were kept until 30 d for tumor metastasis monitoring. The liver and lung tissues harvested from mice received the synergistic immunotherapy showed negligible metastatic foci observed by photographs and H&E staining sections, confirmed the anti-metastasis potential of this combined treatment.

Discussion

PDT can prime “cold” cancer immunotherapy to increase the response rates, but its flexibility is severely limited. To enhancing the therapeutic efficacy of breast cancer, Lp(DHA)@CP Gel was applied to control drug release and therapy tumors. This study demonstrated that Lp(DHA)@CP liposomes in the hydrogel could control the release of αPD-L1 and further improve bioavailability, locally increase drug concentrations, avoid burst drug release, and reduce toxicity and side effects. Meanwhile, hydrogel could be suitable for local drug delivery, protect the integrity of liposomes and improve their stability. The excellent syringe-injectable and self-healing property of Lp(DHA)@CP Gel can be explained by the destruction and reversibly construction of the dynamic Schiff Base bonds between the liposome and hydrogel matrix, which further facilitated the clinical application for *in vivo* injection [43, 44]. The hydrogel was typical of a well-developed network with good mechanical stability, which was favorable for prolonging the retention time at the injection site [45].

The photosensitizer Ce6 encapsulated in liposomal membrane could be triggered by NIR laser to mediate the generation of ROS, which would further cause peroxidation of the unsaturated lipid DHA doped in membrane [46]. The amphipathic DHA molecule could be reversibly oxidized to a complete hydrophilic structure, therefore destabilized the hydrophobic interaction between amphipathic agents to disturb the integrity of the liposome and then allowed the release of encapsulated cargoes [47]. The addition of polyunsaturated fatty acid (DHA) makes the liposomal hydrogel a more a flexible reservoir by enhancing the photoresponsivity. The responsive generation of ROS upon exposure to NIR light disassembled the liposome structure, which would then trigger a spontaneous cascade reaction to release the interior αPD-L1. In particular, in the absence of an initial burst release, Lp(DHA)@CP Gel achieved the sustained controlled release of αPD-L1 *in vitro*, which convinced that the phototriggered drug release property was highly dependent on the existence of ROS-oxidizable unsaturated liposomal membrane materials. This phenomenon was further evidenced by the comparison between liposomal hydrogels with materials of different unsaturation degrees. These results not only illustrated the dependence of photo-responsive

drug release on unsaturated materials, but also underlined the positive corresponding relationships between ROS-responsiveness and unsaturation degrees.

The injectable Lp(DHA)@CP Gel showed outstanding advantages on the convenience of clinical application attributed to its repeatedly-induced therapeutics to after a single implantation, which was beneficial for long-term treatment. Once exposure to laser, Lp(DHA)@C Gel could be more efficient to suppress 4T1 cells and tumors growth due to the induced PDT effect. *In vitro*, the on-demand sustainable release of ROS is a primary cause of cytotoxicity. Such ROS-activated αPD-L1 releasing can subsequently be co-targeted to promote the antitumor immune responses *in vivo*, which was one of the main mechanisms of PDT therapy that could sensitize tumors to ICB therapy [48, 49]. Taken together, these observations unambiguously evidenced the remarkable sustained anticancer efficacy of the one-time implanted Lp(DHA)@CP Gel repeatedly triggered by laser irradiation. Impressively, Lp(DHA)@CP Gel + L was performed almost total ablation of tumors attributed to its PDT effect and the cascaded ICB outcome. This likely occurred because PDT could induce ICD and thus elicit an immune response. Meanwhile, PDT could promote T cell infiltration and increase the proportion of $CD4^+$ and $CD8^+$ T cells [50]. Consequently, this flexible liposome-loaded hydrogel, which facilitated the on-demand photoimmunotherapy then increased therapeutic efficacy while significantly improving patient compliance, has great potential for breast cancer therapy.

Conclusion

In summary, to reduce the medication times and potential overtreatment risks in clinical breast cancer treatment, we have designed a photo-manipulated responsive drug release hydrogel drug delivery platform Lp(DHA)@CP Gel with ROS-responsive disintegrated liposomes cross-linked in it. Abundant ROS was generated by the incorporated Ce6 in response to the NIR light irradiation for PDT, subsequently mediated the disintegrity of liposomal hydrogel for on-demand sustainable release of αPD-L1. Additionally, the generated ROS in TME was also able to sensitize the low-immunogenic “cold” tumors to “hot” by enhancing the T cell infiltration in tumors, thereby increasing their potential responses to ICB drugs. The injected Lp(DHA)@CP Gel completely inhibited the 4T1 tumor growth, and also restrained the recurrence and metastasis of residual tumors. Therefore, the flexible medication platform facilitated repeated photoimmunotherapy after a single dose administration, maximizing the patient compliance and safety by reducing the injection times and adjusting therapeutic behaviors via a photo on-off switch.

Abbreviations

ICB immune checkpoint blockade

PDT photodynamic therapy

αPD-L1 programmed death-ligand 1 antibody

Ce6 photosensitizer chlorin

ICD immunogenic cell death

DHA docosahexaenoic acid

ROS reactive oxygen species

TILs tumor-infiltrating lymphocytes

Tregs regulatory T cells

TAA tumor-associated antigen

Declarations

Acknowledgements

We thank the YM lab members for their valuable contributions to this study.

Authors' contributions

XL and JL designed the experiments and contributed to writing the manuscript. CW, XQ, HL, QX, WL performed the experiments. GY analyzed the data and provided technical support. DZ and MY provided funding and corrections to the manuscript. All authors read and approved the final manuscript.

Funding

This research was supported by Science and Technology Program of Guangzhou (202201011130280065); National Natural Science Foundation of China (82172079); the Research Project of TCM Bureau of Guangdong Province (20231324); Special Fund of Foshan Climbing Peak Plan (2019A004, 2019D039, 2019D041,2020B018).

Availability of data and materials

The datasets used and/or analyzed during the current study are available from the corresponding author on reasonable request.

Ethics approval and consent to participate

All animal studies were conducted in accordance with the Guidelines for the Care and Use of Laboratory Animals of the Institutional Animal Care And Use Committee (IACUC) and were approved by the Animal Ethics Committee of Southern Medical University (SMUL2022187).

Consent for publication

Not applicable.

Competing Interests

All authors declare no competing financial interest.

Author details

[1] School of Pharmaceutical Science Guangdong Provincial Key Laboratory of New Drug Screening Southern Medical University Guangzhou, 510515 China

[2] Zhujiang Hospital, Southern Medical University, Guangzhou, 510282, China

[3] Breast Center, Department of General Surgery, Nanfang Hospital, Southern Medical University, Guangzhou 510515, PR China

[4] Department of Breast Surgery, The First People's Hospital of Foshan, Foshan, 528100, China

[5] Clinical Research Institute, The First People's Hospital of Foshan, Foshan, 528100, China

References

1. H. Sung, J. Ferlay, R.L. Siegel, M. Laversanne, I. Soerjomataram, A. Jemal, F. Bray. Global Cancer Statistics 2020: GLOBOCAN Estimates of Incidence and Mortality Worldwide for 36 Cancers in 185 Countries. CA Cancer J Clin 2021;209-249.
2. H. Zhao, J. Xu, Y. Li, X. Guan, X. Han, Y. Xu, H. Zhou, R. Peng, J. Wang, Z. Liu. Nanoscale Coordination Polymer Based Nanovaccine for Tumor Immunotherapy. ACS nano 2019;13127-13135.
3. Q. Chen, T. Sun, C. Jiang, Recent Advancements in Nanomedicine for 'Cold' Tumor Immunotherapy. Nano-micro letters 2021;92.
4. J.F. Zirkelbach, M. Shah, J. Vallejo, J. Cheng, A. Ayyoub, J. Liu, R. Hudson, R. Sridhara, G. Ison, L.A. Kordestani, S. Tang, T. Gwise, A. Rahman, R. Pazdur, M.R. Theoret. Improving Dose-Optimization Processes Used in Oncology Drug Development to Minimize Toxicity and Maximize Benefit to Patients. Journal of clinical oncology: official journal of the American Society of Clinical Oncology 2022;3489-3500.
5. M. Yi, X. Zheng, M. Niu, S. Zhu, H. Ge, K. Wu. Combination strategies with PD-1/PD-L1 blockade: current advances and future directions. Molecular cancer 2022;28.
6. A.S. Hoffman. Hydrogels for biomedical applications. Advanced drug delivery reviews 2002;3–12.
7. Y. Wang, R.K. Kankala, C. Ou, A. Chen, Z. Yang. Advances in hydrogel-based vascularized tissues for tissue repair and drug screening, Bioactive materials 2021;198-220.
8. S. Correa, A.K. Grosskopf, H.L. Hernandez, D. Chan, A.C. Yu, L.M. Stapleton, E.A. Appel. Translational Applications of Hydrogels. Chemical reviews 2021;11385-11457.
9. E. McAlister, B. Dutton, L.K. Vora, L. Zhao, A. Ripolin, D.S.Z.B.P.H. Zahari, H.L. Quinn, I.A. Tekko, A.J. Courtenay, S.A. Kelly, A.M. Rodgers, L. Steiner, G. Levin, E.L. Nissenbaum, N. Shterman, H.O.

McCarthy, R.F. Donnelly. Directly Compressed Tablets: A Novel Drug-Containing Reservoir Combined with Hydrogel-Forming Microneedle Arrays for Transdermal Drug Delivery. Advanced healthcare materials 2021;2001256.

10. G. Gao, Y.W. Jiang, H.R. Jia, F.G. Wu. Near-infrared light-controllable on-demand antibiotics release using thermo-sensitive hydrogel-based drug reservoir for combating bacterial infection. Biomaterials 2019;83-95.
11. M. Chen, Y. Tan, Z. Dong, J. Lu, X. Han, Q. Jin, W. Zhu, J. Shen, L. Cheng, Z. Liu, Q. Chen. Injectable Anti-inflammatory Nanofiber Hydrogel to Achieve Systemic Immunotherapy Post Local Administration. Nano letters 2020;6763-6773.
12. L. Huang, Y. Li, Y. Du, Y. Zhang, X. Wang, Y. Ding, X. Yang, F. Meng, J. Tu, L. Luo, C. Sun. Mild photothermal therapy potentiates anti-PD-L1 treatment for immunologically cold tumors via an all-in-one and all-in-control strategy. Nature communications 2019;4871.
13. H. Cabral, H. Kinoh, K. Kataoka. Tumor-Targeted Nanomedicine for Immunotherapy. Accounts of chemical research 2020;2765-2776.
14. F. Wang, H. Su, R. Lin, R.W. Chakroun, M.K. Monroe, Z. Wang, M. Porter, H. Cui. Supramolecular Tubustecan Hydrogel as Chemotherapeutic Carrier to Improve Tumor Penetration and Local Treatment Efficacy. ACS nano 2020;10083-10094.
15. V. Yesilyurt, A.M. Ayoob, E.A. Appel, J.T. Borenstein, R. Langer, D.G. Anderson. Mixed Reversible Covalent Crosslink Kinetics Enable Precise, Hierarchical Mechanical Tuning of Hydrogel Networks. Advanced materials 2017;1605947.
16. V.G. Muir, J.A. Burdick. Chemically Modified Biopolymers for the Formation of Biomedical Hydrogels. Chemical reviews 2021;10908-10949.
17. A.Y. Rwei, J.J. Lee, C. Zhan, Q. Liu, M.T. Ok, S.A. Shankarappa, R. Langer, D.S. Kohane. Repeatable and adjustable on-demand sciatic nerve block with phototriggerable liposomes. Proceedings of the National Academy of Sciences of the United States of America 2015;15719-15724.
18. H. Xu, P. She, B. Ma, Z. Zhao, G. Li, Y. Wang. ROS responsive nanoparticles loaded with lipid-specific AIEgen for atherosclerosis-targeted diagnosis and bifunctional therapy. Biomaterials 2022;121734.
19. Q. Xu, G. Chen, G. Chen, H. Wu, Y. Yang, Z. Mai, R. Sun, P. Luan, C. Guo, M. Yu, Z. Peng, Z. Yu. NO-dependent vasodilation and deep tumor penetration for cascade-amplified antitumor performance. J. Control. Release 2022;389-399.
20. I.S. Kim, Y. Gao, T. Welte, H. Wang, J. Liu, M. Janghorban, K. Sheng, Y. Niu, A. Goldstein, N. Zhao, I. Bado, H.C. Lo, M.J. Toneff, T. Nguyen, W. Bu, W. Jiang, J. Arnold, F. Gu, J. He, D. Jebakumar, K. Walker, Y. Li, Q. Mo, T.F. Westbroo, C. Zong, A. Rao, A. Sreekumar, J.M. Rosen, X.H. Zhang. Immuno-subtyping of breast cancer reveals distinct myeloid cell profiles and immunotherapy resistance mechanisms. Nature cell biology 2019;1113-1126.
21. S. Adams, M.E.G. Mays, K. Kalinsky, L.A. Korde, E. Sharon, L.A. Kordestani, H. Bear, H. L. McArthur, E. Frank, J. Perlmutter, D.B. Page, B. Vincent, J.F. Hayes, J.L. Gulley, J.K. Litton, G.N. Hortobagyi, S. Chia,

I. Krop, J. White, J. Sparano, M.L. Disis, E.A. Mittendorf. Current Landscape of Immunotherapy in Breast Cancer: A Review. JAMA oncology 2019;1205-1214.

22. A. Bassez, H. Vos, L.V. Dyck, G. Floris, I. Arijs, C. Desmedt, B. Boeckx, M.V. Bempt, I. Nevelsteen, K. Lambein, K. Punie, P. Neven, A.D. Garg, H. Wildiers, J. Qian, A. Smeets, D. Lambrechts. A single-cell map of intratumoral changes during anti-PD1 treatment of patients with breast cancer. Nature medicine 2021;820-832.
23. E. Masoumi, S.T. Hajghorbani, L. Jafarzadeh, M.J. Sanaei, A.P. Sigaroodi, D. Bashash. The application of immune checkpoint blockade in breast cancer and the emerging role of nanoparticle. J. Control. Release 2021;168-187.
24. S. Wang, Z. Wang, Z. Li, J. Xu, X. Meng, Z. Zhao, Y. Hou. A Catalytic Immune Activator Based on Magnetic Nanoparticles to Reprogram the Immunoecology of Breast Cancer from "Cold" to "Hot" State. Advanced healthcare materials 2022;e2201240.
25. T. Wang, Z. Gao, Y. Zhang, Y. Hong, Y. Tang, K. Shan, X. Kong, Z. Wang, Y. Shi, D. Ding. A supramolecular self-assembled nanomaterial for synergistic therapy of immunosuppressive tumor. J. Control Release 2022;272-283.
26. Y. Zhang, S. Tian, L. Huang, Y. Li, Y. Lu, H. Li, G. Chen, F. Meng, G. L. Liu, X. Yang, J. Tu, C. Sun, L. Luo. Reactive oxygen species-responsive and Raman-traceable hydrogel combining photodynamic and immune therapy for postsurgical cancer treatment. Nature communications 2022;4553.
27. J. Zhang, D. Huang, P.E. Saw, E. Song. Turning cold tumors hot: from molecular mechanisms to clinical applications. Trends in immunology 2022;523-545.
28. M.F. Attia, N. Anton, J. Wallyn, Z. Omran, T.F. Vandamme. An overview of active and passive targeting strategies to improve the nanocarriers efficiency to tumour sites. J. Pharm Pharmacol 2019;1185-1198.
29. V. Sunil, J.H. Teoh, B.C. Mohan, A. Mozhi, C.H. Wang. Bioengineered immunomodulatory organelle targeted nanozymes for photodynamic immunometabolic therapy. J. Control Release 2022;215-227.
30. R. Guo, S. Wang, L. Zhao, Q. Zong, T. Li, G. Ling, P. Zhang. Engineered nanomaterials for synergistic photo-immunotherapy. Biomaterials 2022;121425.
31. Y. Zhao, Z. Chen, Q. Li, X. Cao, Q. Huang, L. Shi, Y. Liu. Polymer-Reinforced Liposomes Amplify Immunogenic Cell Death-Associated Antitumor Immunity for Photodynamic-Immunotherapy. Adv. Funct. Mater 2022;2209711.
32. H.E. Barash, I. Shichor, A.H. Kwon, S. Hall, M.W. Lawlor, R. Langer, D.S. Kohane. Prolonged duration local anesthesia with minimal toxicity. Proc Natl Acad Sci USA 2009;7125–7130.
33. H. Ren, Y. He, J. Liang, Z. Cheng, M. Zhang, Y. Zhu, C. Hong, J. Qin, X. Xu, J. Wang. Role of Liposome Size, Surface Charge, and PEGylation on Rheumatoid Arthritis Targeting Therapy. ACS Appl Mater Interfaces 2019;20304–20315.
34. Y. Gao, K. Peng, S. Mitragotri. Covalently Crosslinked Hydrogels via Step-Growth Reactions: Crosslinking Chemistries, Polymers, and Clinical Impact. Adv Mater 2021;e2006362.

35. H. Lin, S. Shi, X. Lan, X. Quan, Q. Xu, G. Yao, J. Liu, X. Shuai, C. Wang, X. Li, M. Yu. Scaffold 3D-Printed from Metallic Nanoparticles-Containing Ink Simultaneously Eradicates Tumor and Repairs Tumor-Associated Bone Defects. Small methods 2021;e2100536.
36. H. Zhang, X. Yong, J. Zhou, J. Deng, Y. Wu. Biomass Vanillin-Derived Polymeric Microspheres Containing Functional Aldehyde Groups: Preparation, Characterization, and Application as Adsorbent. ACS Appl Mater Interfaces 2016;10951-10953.
37. J. Kiwi, V. Nadtochenko. New evidence for TiO2 photocatalysis during bilayer lipid peroxidation. J. J Phys Chem B 2004;2499-2506.
38. S.O. Gollnick. Photodynamic therapy and antitumor immunity. J Natl Compr Canc Netw 2012;2753-2763.
39. R. Mahjub, S. Jatana, S.E. Lee, Z. Qin, G. Pauli, M. Soleimani, S. Madadi, S.D. Li. Recent advances in applying nanotechnologies for cancer immunotherapy. J Control Release 2018;2037-2044.
40. L.D. Church, G.P. Cook, M.F. McDermott. Primer: inflammasomes and interleukin 1beta in inflammatory disorders. Nat Clin Pract Rheumatol 2008;715S-725S.
41. A. Kalbasi, A. Ribas. Tumour-intrinsic resistance to immune checkpoint blockade. Nat Rev Immunol 2020.
42. Y. Qiu, T. Chen, R. Hu, R. Zhu, C. Li, Y. Ruan, X. Xie, Y. Li. Next frontier in tumor immunotherapy: macrophage-mediated immune evasion. Biomark Res 2021;2849-2864.
43. C.T. Huynh, M.K. Nguyen, D.S. Lee. Dually cationic and anionic pH/temperature-sensitive injectable hydrogels and potential application as a protein carrier. Chem Commun (Camb) 2012;121833.
44. H. Tan, C.R. Chu, K.A. Payne, K.G. Marra. Injectable in situ forming biodegradable chitosan-hyaluronic acid based hydrogels for cartilage tissue engineering. Biomaterials 2009;1276-1288.
45. Y. Ma, J. Yang, B. Li, Y. J, X. Lu, Z. Chen. Biodegradable and injectable polymer–liposome hydrogel: a promising cell carrier. Polymer Chemistry 2016;S40-S43.
46. B. Halliwell, S. Chirico. Lipid peroxidation: its mechanism, measurement, and significance. Am J Clin Nutr 1993;239-263.
47. Y. Wang, H. Xu, X. Zhang. Tuning The Amphiphilicity Of Building Blocks: Controlled Self-Assembly And Disassembly For Functional Supramolecular Materials. Adv Mater 2009;653-663.
48. H.Z. Xu, T.F. Li, Y. Ma, K. Li, Q. Zhang, Y.H. Xu, Y.C. Zhang, L. Zhao, X. Chen. Targeted photodynamic therapy of glioblastoma mediated by platelets with photo-controlled release property. Biomaterials 2022;34-42.
49. C.J. Liu, M. Schaettler, D.T. Blaha, J.A.B. Kirigin, D.K. Kobayashi, A.J. Livingstone, D. Bender, C.A. Miller, D.M. Kranz, T.M. Johanns, G.P. Dunn. Treatment of an aggressive orthotopic murine glioblastoma model with combination checkpoint blockade and a multivalent neoantigen vaccine. Neuro Oncol 2020;25-39.
50. M. Firczuk, D. Nowis, J. Gołąb. PDT-induced inflammatory and host responses. Photochem Photobiol Sci 2011;72.

Schemes

Scheme 1 is available in the Supplementary Files section

Figures

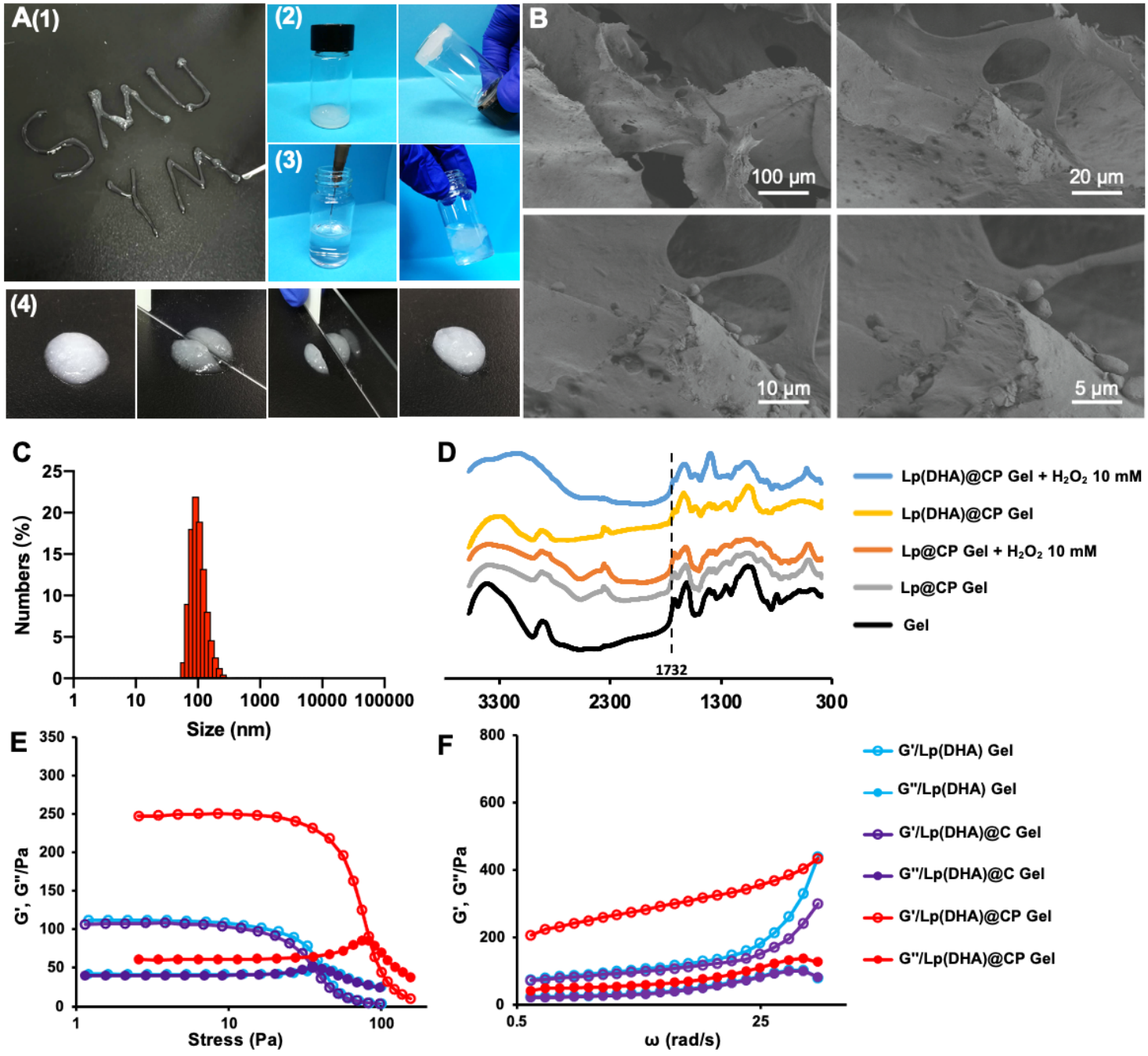

Figure 1

Synthesis and characterization of the Lp(DHA)@CP Gel. (A) Injectable and self-healing capabilities of the liposomal hydrogel evaluated by extruding through a syringe (1), upside-down storage (2), morphological stability in water (3), and cut-recovery study (4). (B) Representative SEM images of the freeze-dried

Lp(DHA)@CP Gel. (C) Particle size distribution of the Lp(DHA)@CP. (D) FTIR spectra of the Lp(DHA)@CP Gel. Storage modulus *G'* and loss modulus *G"* of the Lp(DHA)@CP Gel at different stress (E) and frequency (F) at 37 °C.

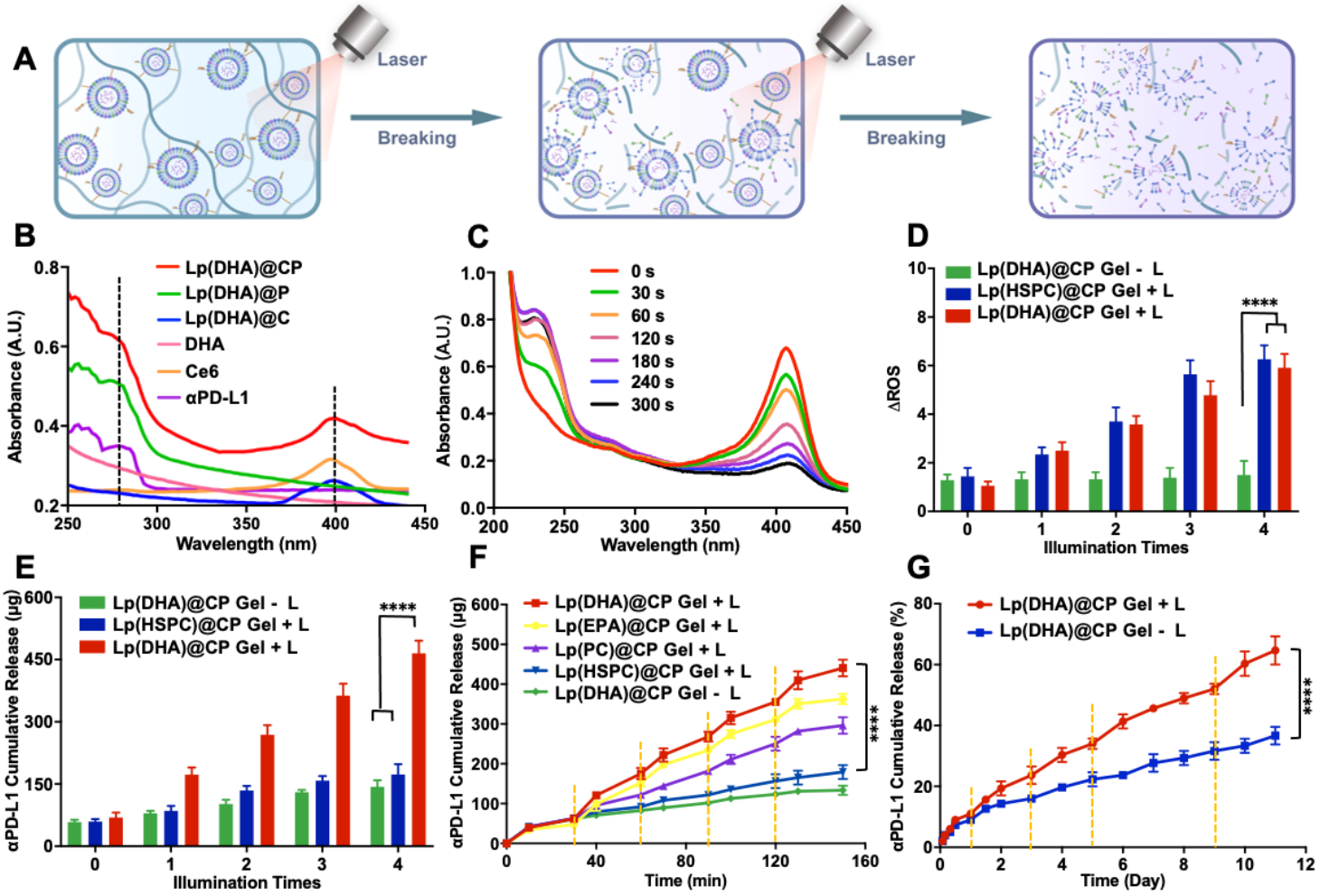

Figure 2

Photo-triggered ROS generation and the cascaded αPD-L1 release. (A) Schematic of Photo-triggered cargo release from liposome hydrogels. (B) UV–vis spectra of different liposomes. (C) Absorption spectra of Lp(DHA)@CP Gel under laser exposure for different time periods (671 nm, 100 mW/cm^2) in PBS. Cumulative ROS production (D) and corresponding αPD-L1 release (E) from different liposome hydrogels triggered by laser irradiation (671 nm, 100 mW/cm^2) for different times. Short-term (F) and long term (G) responsive release of αPD-L1 from liposome hydrogels at 37 °C with and without laser irradiation (671 nm, 100 mW/cm^2, 3 min) at different time points indicated by dotted lines.

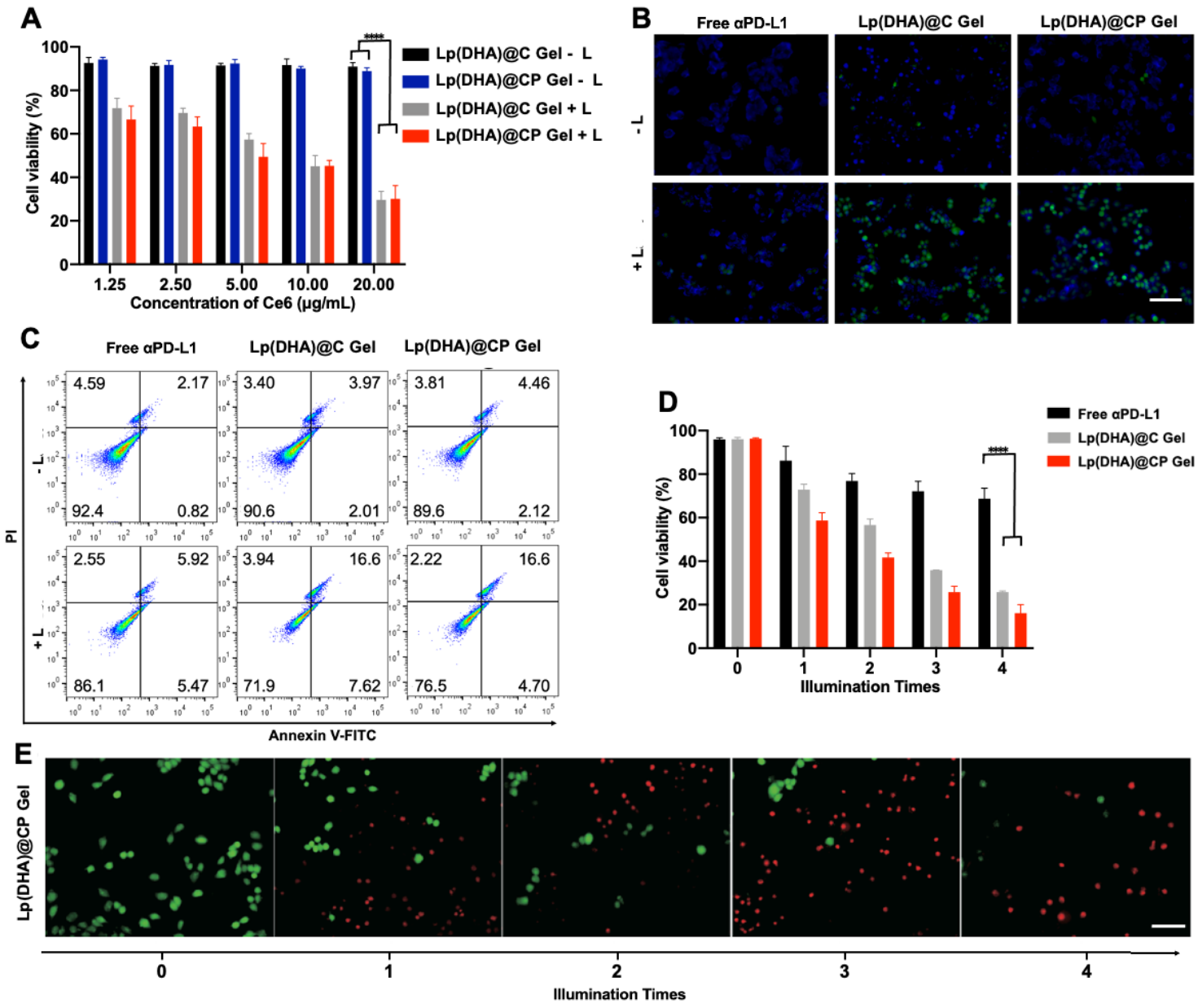

Figure 3

Photo-triggered cytotoxicity of Lp(DHA)@CP Gel. (A) Cytotoxicity of liposome hydrogels on 4T1 cells with or without laser irradiation. (B) ROS generation in 4T1 cells after different treatments with or without NIR laser irradiation (671 nm, 100 mW/cm^2, 3 min) determined by CLSM observation using DCFH-DA kit. Scale bar: 100 μm. (C) Cell apoptosis of 4T1 cells after different treatments with or without laser irradiation (671 nm, 100 mW/cm^2, 3 min) determined by flow cytometry. (D) Cytotoxicity of hydrogels on 4T1 cells with laser irradiation for different times. (E) CLSM observation of photo-triggered cytotoxicity of Lp(DHA)@CP Gel on 4T1 tumor cells after laser irradiation for different times. The live and dead cells were stained by Calcein AM (green) and propidium iodide (red), respectively. Scale bar: 100 μm.

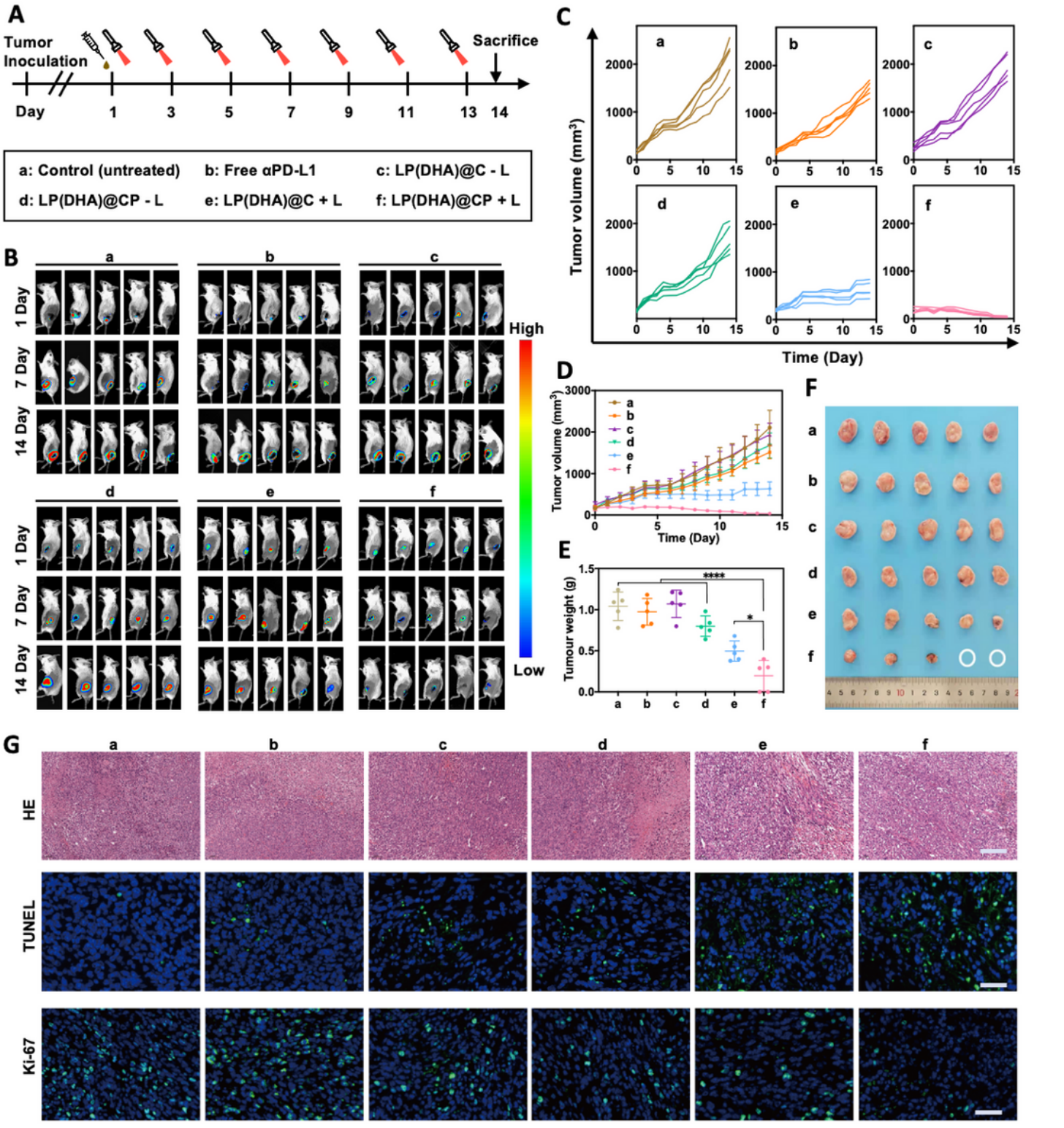

Figure 4

Antitumor performance of Lp(DHA)@CP Gel by photo-triggering PDT and the cascaded immune therapy effect. (A) Schematic illustration of the antitumor experimental design. (B) Representative *in vivo* bioluminescence images of 4T1 tumor-bearing mice treated with liposome hydrogels at different time points.Primary tumor growth curves of individual mouse (C) and average tumor volumes (D) in different groups of 4T1 tumor–bearing BALB/c mice model. (n = 5). The weights (E) and photographs (F) of *ex*

vivo tumors from different treated mice executed on 14 d. (G) H&E, TUNEL and immunohistochemistry staining of tumor sections from mice receiving various hydrogel-treatments. Scale bar: 100 μm.

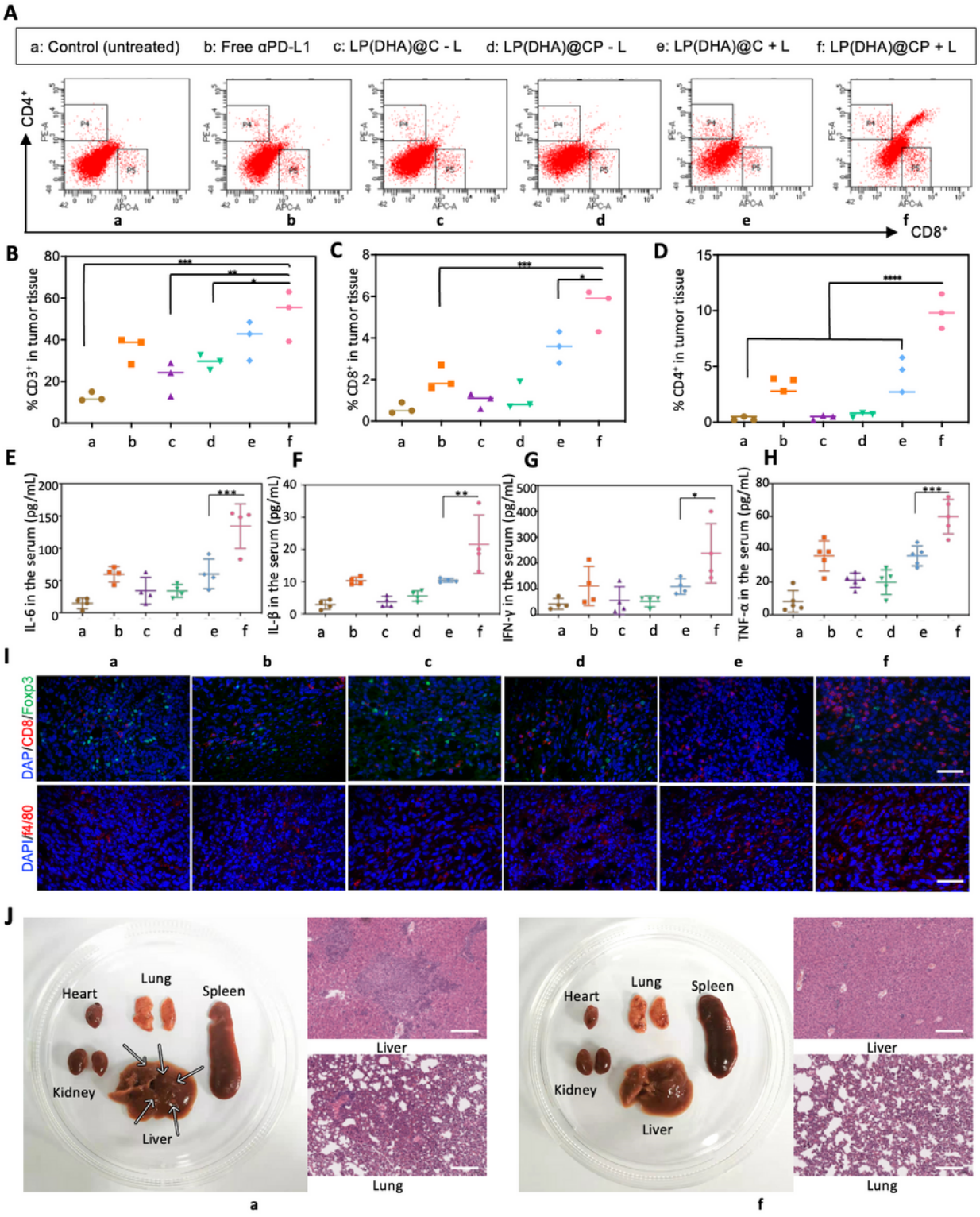

Figure 5

In vivo immune response regulated by Lp(DHA)@CP Gel and long-term anti-metastasis effect. (A) Infiltration of $CD8^+$ TILs ($CD3^+$ $CD8^+$) in the tumor tissues collected from mice after various treatments

analyzed by flow cytometry. Frequency of tumor-infiltrating $CD3^+$ T cells (B), $CD8^+$ T cells (C) and $CD4^+$ T cells (D). Levels of cytokines including IL-6 (E), IL-1β (F), IFN-γ (G) and TNF-α (H) in serum from mice after various treatments measured by ELISA assay. (I) Immunofluorescence assays of $CD8^+$ T cell and macrophages in tumor tissues from mice after various treatments. Scale bar: 100 μm. (J) Long-term anti-metastasis effect of Lp(DHA)@CP Gel evaluated by photographs of major organs and H&E staining of liver and lung sections from 4T1 tumor-bearing mice at 30 d after treatment. Metastatic foci were indicated by arrows. Scale bar: 100 μm.

Supplementary Files

This is a list of supplementary files associated with this preprint. Click to download.

- Scheme1.png
- BiomaterialResearchSI.02.12.docx
- AuthorChecklistl.pdf